



# Assembly of Copper Phthalocyanine on TiO<sub>2</sub> Nanorod Arrays as Co-catalyst for Enhanced Photoelectrochemical Water Splitting

Yuangang Li<sup>1,2\*</sup>, Mengru Yang<sup>1</sup>, Zimin Tian<sup>1</sup>, Ningdan Luo<sup>1</sup>, Yan Li<sup>3</sup>, Haohao Zhang<sup>1</sup>, Anning Zhou<sup>1,2</sup> and Shanxin Xiong<sup>1,2\*</sup>

<sup>1</sup> College of Chemistry and Chemical Engineering, Xi'an University of Science and Technology, Xi'an, China, <sup>2</sup> Key Laboratory of Coal Resources Exploration and Comprehensive Utilization, Xi'an, China, <sup>3</sup> Key Laboratory of Synthetic and Natural Functional Molecule Chemistry of the Ministry of Education, College of Chemistry and Materials Science, Northwest University, Xi'an, China

## OPEN ACCESS

### Edited by:

Penglei Chen,  
Institute of Chemistry (CAS), China

### Reviewed by:

Zhiyong Tang,  
National Center for Nanoscience and  
Technology (CAS), China

Bin Chen,

Technical Institute of Physics and  
Chemistry (CAS), China

Jiahai Ma,

University of Chinese Academy of  
Sciences (UCAS), China

### \*Correspondence:

Yuangang Li  
liyurangang@xust.edu.cn  
Shanxin Xiong  
xiongsx@xust.edu.cn

### Specialty section:

This article was submitted to  
Supramolecular Chemistry,  
a section of the journal  
Frontiers in Chemistry

**Received:** 21 December 2018

**Accepted:** 24 April 2019

**Published:** 14 May 2019

### Citation:

Li Y, Yang M, Tian Z, Luo N, Li Y,  
Zhang H, Zhou A and Xiong S (2019)  
Assembly of Copper Phthalocyanine  
on TiO<sub>2</sub> Nanorod Arrays as  
Co-catalyst for Enhanced  
Photoelectrochemical Water Splitting.  
Front. Chem. 7:334.  
doi: 10.3389/fchem.2019.00334

A photoelectrochemical device was achieved by interfacial self-assembly of macrocyclic  $\pi$ -conjugated copper phthalocyanine (CuPc) on surface of TiO<sub>2</sub> nanorod arrays (NRs). The photocurrent density of the elegant TiO<sub>2</sub>@CuPc NRs photoanode reaches 2.40 mA/cm<sup>2</sup> at 1.23 V vs. RHE under the illumination of 100 mW/cm<sup>2</sup> from AM 1.5G sun simulator, which is 2.4 times higher than that of the pure TiO<sub>2</sub>. At the same time, the photoelectrochemical device constructed through this strategy has good stability and the photocurrent density remain almost no decline after 8 h of continuous operation. The Mott-Schottky and LSV curves demonstrate that CuPc act as a co-catalyst for water oxidation and a possible mechanism is proposed for water oxidation based on careful analysis of the detailed results. The holes from VB of TiO<sub>2</sub> photogenerated by electrons exciting are consumed by a process in which Cu<sup>2+</sup> is oxidized to Cu<sup>3+</sup> and Cu<sup>4+</sup>, and then oxidize water to produce oxygen. CuPc species is considered to be a fast redox mediator to reduce the activation energy of water oxidation in and effectively promote charge separation.

**Keywords:** self-assembly, copper phthalocyanine, TiO<sub>2</sub>, water oxidation, surficial nanostructure

## INTRODUCTION

Photoelectrochemical (PEC) water splitting is considered as one of the most promising technologies to address the challenges of impending worldwide energy consuming and associated climate change resulting from combustion of fossil fuels (Du and Eisenberg, 2012; Wang et al., 2016; Seh et al., 2017). Through this promising strategy, hydrogen could be produced as a clean fuel by sun light photolysis of water under the help of a bias potential (Ferreira et al., 2004; Gibson et al., 2017; Li et al., 2017). However, the sluggish kinetics of the two half-reactions of water splitting, especially the more sluggish four-electron oxygen evolution reaction, always leads to poor performance of the PEC device and relatively low energy efficiency (Haumann et al., 2005; Bessel et al., 2010; Fang et al., 2017). Therefore, many research works in the past have still focused on the design and improving the performance of photo anode on which water oxidation occurred, although the more desired hydrogen evolution reaction occurred on the photo cathode (Osterloh, 2013; Meyer et al., 2017). In order to achieve PEC device with relatively high performance, many

strategies have been employed. One of the effective strategies is adopting photo electrode of vertically aligned arrays (Lee and Chen, 2014) compositing of low dimensional nanostructures such as nanorods (Bin and Aydil, 2009; Liu B. et al., 2013; Li et al., 2016b; Tang et al., 2017), nanowires (Hang et al., 2001; Li et al., 2016a; Zhang et al., 2016; Jeong et al., 2018; Yao et al., 2018), and nanosheets (Zhu et al., 2011; Yang et al., 2012; Du et al., 2013; Zhang et al., 2014; Zhang R. et al., 2018; Shi et al., 2018; Zhao et al., 2018a) because this kind of interfacial nanostructures can decouple the length scales of charge diffusion and light absorption, at the same time offering sufficient surface area for the photogenerated electrons or holes to diffuse onto the interface of electrolyte and electrode (Xiao et al., 2015). TiO<sub>2</sub> nanorod arrays (Akira and Kenichi, 1972; Liu L. et al., 2013; Li et al., 2015, 2016c) had been applied extensively in PEC water splitting as for its low cost, non-toxic, and stable performance.

Another effective way is selecting a suitable co-catalyst to improve the photo electrochemical performance and water oxidation activity in the process of assembling photo electrochemical device (Ran et al., 2014; Ding et al., 2017; Zhang Y. et al., 2018). In the process of PEC water splitting, co-catalysts play three pivotal roles for improving the reliability and activity of semiconductor: (i) co-catalysts could reduce the over-potential (Artero et al., 2011) or activation energy for oxygen production reactions on the surface of semiconductors; (ii) co-catalysts are capable of slowing electron-hole recombination at the interface between co-catalyst and semiconductor; (iii) co-catalysts could improve the stability of semiconductor photo electrode and suppress the photo-corrosion. Over the past few years, the advances of electrode manufacturing technology and materials science have greatly expanded in O<sub>2</sub> evolution (Li et al., 2012; Nepal and Das, 2013; Lauinger et al., 2015; Gong et al., 2016). Many kinds of novel co-catalysts and interlayers were successfully loaded on various photoelectrodes (Long et al., 2018; Zhao et al., 2018b; Yin et al., 2019). Thus far, noble-metal oxides (IrO<sub>2</sub> or RuO<sub>2</sub>) act as the best accepted O<sub>2</sub>-evolution co-catalysts, which have lower over-potential for oxygen evolution in acidic conditions (Junya et al., 2005; Blakemore et al., 2010; Cherevko et al., 2015).

With the exception of rare and precious metals, some noble-metal-free and low-cost transitional metals, such as Co (Youn et al., 2015; Zhang et al., 2017), Ni (Yoon et al., 2015) and Fe (Youn et al., 2015) have also been used as co-catalysts in PEC O<sub>2</sub> production. Although copper (Zhou et al., 2015) based catalyst often has been applied for H<sub>2</sub> evolution (Kumar et al., 2016), hardly for O<sub>2</sub> production (Terao et al., 2016; Chauhan et al., 2017), in Lu group (Lu et al., 2016), Cu(II) aliphatic diamine complexes was immobilized on ITO as heterogeneous water oxidation catalysts. In Su (Su et al., 2015) and Zhang (Zhang et al., 2013) group, copper complexes were synthesized as homogeneous O<sub>2</sub> production catalysts. Copper phthalocyanine is a kind of organic heterocyclic compounds, containing large ring  $\Pi$  conjugated structure with good stability and effective property (Jiang et al., 2017).

It has been proven that supramolecular self-assembly of  $\pi$ -conjugated molecules was a good strategy to fabricate various functional organic-based nanostructured materials, which

aims to manufacturing sophisticated organized molecular aggregate, through various non-covalent interactions, including hydrophobic interactions,  $\pi$ - $\pi$  interactions, electrostatic interactions, etc. (Chen et al., 2008; Zhang et al., 2009; Qiu et al., 2010; Guo et al., 2011, 2012). Although, supramolecular assembled nanostructures (Wang et al., 2014; Liu et al., 2015; Geng et al., 2018) based on  $\pi$ -conjugated phthalocyanine derivatives have been reported to be effective in the field of laser printing, xerography, organic solar cells, etc., it is very rare to apply this kind of strategy for constructing PEC device. Herein, we adopted an electro-induced surficial assembly method to construct PEC device with enhanced performance. We employ copper phthalocyanine (CuPc) as an O<sub>2</sub> evolution co-catalyst and TiO<sub>2</sub> nanorod arrays (TNRAs) as semiconductor for light harvesting. The obtained surficial nanostructured assembly could be used as photo anode for efficient PEC water splitting. The photocurrent density of the elegant CuPc assembled TiO<sub>2</sub> nanorod arrays (CTNRAs) photoanode reaches 2.4 mA/cm<sup>2</sup> at 1.23 V vs. RHE, which is more than 2 folds higher than that of the pristine TNRAs and the stability of the PEC device is also very good. There have no obvious performance decline after 8 h continuous operation. A possible mechanism for PEC water oxidation on CTNRAs was proposed based on detailed experiments.

## EXPERIMENTAL SECTION

### Sample Preparation

#### Materials

All chemicals were analytical grade and used without further treatment. Fluorine-doped tin oxide (FTO) substrates (14  $\Omega$ /square) were obtained from Huanan Xiangcheng Technology Co., Ltd. Copper phthalocyanine (C<sub>32</sub>H<sub>16</sub>CuN<sub>8</sub>), tetrabutyl titanate (C<sub>16</sub>H<sub>36</sub>O<sub>4</sub>Ti), Trifluoroacetic acid (CF<sub>3</sub>COOH), and methanol (CH<sub>3</sub>OH) were purchased from Aladdin Chemical Reagent Co. Ltd. In addition, acetone (C<sub>3</sub>H<sub>6</sub>O), hydrochloric acid (HCl), and absolute ethanol (C<sub>2</sub>H<sub>5</sub>OH) were bought from Sinopharm Chemical Reagent Co. Ltd. Ultrapure water was used in the experiments.

#### Preparation of FTO@TiO<sub>2</sub> (TNRAs) and FTO@TiO<sub>2</sub>@CuPc (CTNRAs)

**Preparation of TNRAs** TiO<sub>2</sub> nanorod arrays were prepared by hydrothermal method in autoclave (Bin and Aydil, 2009). Firstly, FTO were cleaned ultrasonically three times in solvents of acetone, ethanol and deionized water alternatively 15 min per step, and were dried in vacuum dryer at 60°C. Next, 0.4 mL tetrabutyl titanate were added drop wise into uniform mixed solution of 12 mL ultrapure water and 12 mL hydrochloric acid (mass fraction 36.5–38 %). When the mixture solution of precursor was clarified, we transferred it into 100 mL of Teflon-lined stainless steel autoclave. The conductive surface of FTO was put downwards at a slight angle with the inner wall of autoclave. Then, the autoclave was kept in an oven of 150°C for 15 h and cooled to 25°C. Then the FTO with nanorod arrays of TiO<sub>2</sub> were taken out and dried. Finally, the TiO<sub>2</sub> nanorod arrays were annealed at 450°C for 1 h.

**Preparation of CTNRAs** For synthesis of CTNRAs, 3  $\mu\text{mol}$  CuPc were dissolved in 5 mmol trifluoroacetic acid, which mixed with 50 mL chloroform as electroplate solution (Ogunsipe and Nyokong, 2004). The mono-protonated  $[\text{CuPc}\cdot\text{H}]^+$  (Figure S1A) and di-protonated  $[\text{CuPc}\cdot\text{H}_2]^{2+}$  (Figures S1B,C) forms of copper phthalocyanine (CuPc) were obtained by TFA (Su et al., 2009). The CTNRAs was fabricated by the electrophoretic deposition (EPD) method from the protonated CuPc dissolved in chloroform containing TFA. Then The  $\text{CuPc}^+$  ( $[\text{CuPc}\cdot\text{H}]^+$  and  $[\text{CuPc}\cdot\text{H}_2]^{2+}$ ) was loaded on TNRAs by electrodeposition of 30, 60, 90, 120, and 150 s. Next  $\text{CuPc}^+$  were deprotonated by dipping the TNRAs substrate in 1 M ammonia for 1 h and drying for 1 h at  $200^\circ\text{C}$  and CuPc was successfully covered onto  $\text{TiO}_2$  nanorod arrays (Figure 1). FTO@CuPc was prepared in the same way.

## Materials Characterizations

XRD were characterized by a Shimadzu 7000S X-ray diffractometer with  $\text{Cu}\text{-K}\alpha$  radiation and operating in a  $2\theta$  range of  $20\text{--}70^\circ$  at a scan rate of  $5^\circ$  per minute. XPS patterns of the as-prepared samples were carried on a Kratos Axis Ultra DLD system with an Al  $\text{K}\alpha$  X-ray source ( $h\nu = 1486.69\text{ eV}$ ). The morphologies, EDS mapping analyse and high-resolution images were studied by a field emission Tecnai G2 F20 transmission electron microscopy with an acceleration voltage of 200 kV. SEM images were achieved using a Hitachi S-4800 field-emission scanning electron microscopy. Raman spectra were investigated on a WITec Alpha 300 R Confocal Raman Spectrometer, which has an excitation wavelength of 532 nm at the room temperature. The UV-vis spectra were characterized by a Shimadzu UV-2550 UV-Vis spectrophotometer using  $\text{BaSO}_4$  as the reference. The linear sweep voltammetry (LSV), electrochemical impedance spectroscopy (EIS) and cycle voltammetry (CV) were conducted using an electrochemical workstation (CHI 660E) in a three-electrode system. The incident photon-to-current conversion efficiency (IPCE) was measured by the same workstation and a Xenon lamp (300 W) coupled with a monochromator. Inductively coupled plasma (ICP) measurement was carried on Varian 715-ES.

## PEC Measurements

PEC water oxidation was investigated using a three-electrode potential station (CHI 660 E, China) with a saturated  $\text{Ag}/\text{AgCl}$  (in 3 M KCl) as reference electrode and a platinum wire as counter electrode. The schematic illustration for the geometry and design of PEC reactor was shown in Figure S16. Under AM 1.5G simulated solar light illumination ( $100\text{ mW}/\text{cm}^2$ ) from a Xe lamp (300 W), the as-prepared working electrodes exhibit photoelectron activity for water splitting. 0.1 M sodium sulfate solution ( $\text{pH} \approx 6.8$ ) was used as electrolyte with 30 min  $\text{N}_2$  bubbling. LSV was conducted at a scan rate of 10 mV/s. The potential of the working electrodes (vs.  $\text{Ag}/\text{AgCl}$ ) can be converted to the reversible hydrogen electrode (RHE) by the Nernst equation:

$$E_{\text{RHE}} = E_{\text{Ag}/\text{AgCl}} + 0.0591\text{pH} + 0.19742$$

## RESULT AND DISCUSSION

TNRAs on FTO were prepared in an autoclave by a hydrothermal method. The obtained TNRAs are almost vertically grown on the FTO substrate, with an average diameter and length of  $\sim 500\text{ nm}$  and  $\sim 3\ \mu\text{m}$ , respectively (Figure 2A and Figure S4A). Each nanorod consisted of several smaller rods as shown in Figure S1C. Transmission electron microscopy picture from a single nanorod (Figure 2C, and Figures S2A,B) shown that the diameter observed is about  $600\text{--}800\text{ nm}$  which is in accordance with SEM observation. High-resolution transmission electron microscopy (HR-TEM) of TNRAs showed that two kinds of lattice fringes could be clearly observed and the distances between adjacent lattice fringes were about  $0.325$  and  $0.249\text{ nm}$  (Figure 2E), respectively. After careful comparison with the results of literature we attribute them as lattice fringes from the crystal lattice of (110) and (101) of rutile  $\text{TiO}_2$ , respectively, illustrating that the obtained TNRAs is rutile  $\text{TiO}_2$  and grow along with the direction of (001) lattice (Wang et al., 2011).

The CTNRAs were fabricated through a simple electrodeposition method, as illustrated in Figure 1. The SEM images of CTNRAs were almost the same as pure TNRAs (Figure 2B and Figures S3C, S4B), which indicate the process of the CuPc deposition does not damage the structure of the pristine TNRAs. But from Figure 2D and Figure S3 we can observe that the surface of  $\text{TiO}_2$  was more rough compared with that of TNRAs. The HR-TEM of CTNRAs reveals a single crystalline structure in Figure 2F. Lattice fringes of  $0.147\text{ nm}$  (002),  $0.167\text{ nm}$  (211), and  $0.249\text{ nm}$  (101) belong to rutile  $\text{TiO}_2$  and which is consistent with that of pure TNRAs. Although the lattice structure of CuPc was not found, the characteristic elements of nitrogen and copper of CuPc could be seen in energy dispersive X-ray elemental mapping (Figures 2G,H). From the elemental mapping images of CTNRAs as shown in Figure 2G, it is observed that the copper and nitrogen elements from CuPc distribute as uniformly as the elements of oxygen and titanium from  $\text{TiO}_2$ , which means that CuPc was successfully deposited on the surface of TNRAs and the deposited CuPc distribute uniformly on the whole surface of  $\text{TiO}_2$  nanorod.

X-ray diffraction (XRD) curves (Figure 3A) indicate that both TNRAs and CTNRAs can be ascribed to the tetragonal  $\text{TiO}_2$  with the rutile phase (JCPDS 21-1276). As for pristine  $\text{TiO}_2$ , the main distinct diffraction peaks at  $36.3^\circ$ ,  $54.5^\circ$ , and  $62.6^\circ$  can be well attributed to (101), (211), and (002) crystal planes, respectively. The XRD spectra are consistent with HR-TEM patterns. The other distinct diffraction peaks from TNRAs located at  $2\theta$  values of  $27.2^\circ$ ,  $33.7^\circ$ ,  $38.1^\circ$ ,  $57.1^\circ$ , and  $66.2^\circ$  are attributed to  $\text{SnO}_2$  from FTO substrate. No apparent peaks of CuPc can be observed in CTNRAs samples due to the low loading of CuPc, or the amorphous state of CuPc from electrodeposition method.

Raman spectroscopy measurements were employed to further observe the existence of CuPc on the surface of CTNRAs. The data shown in Figure 3B clearly proved that CuPc was successfully deposited on TNRAs to form CTNRAs. The spectrum of pristine TNRAs show four characteristic peaks at  $143$ ,  $448$ ,  $608$ , and  $238\text{ cm}^{-1}$ , respectively, matching well with the B1g, Eg, A1g of rutile  $\text{TiO}_2$  and lattice distortion or multi spectral

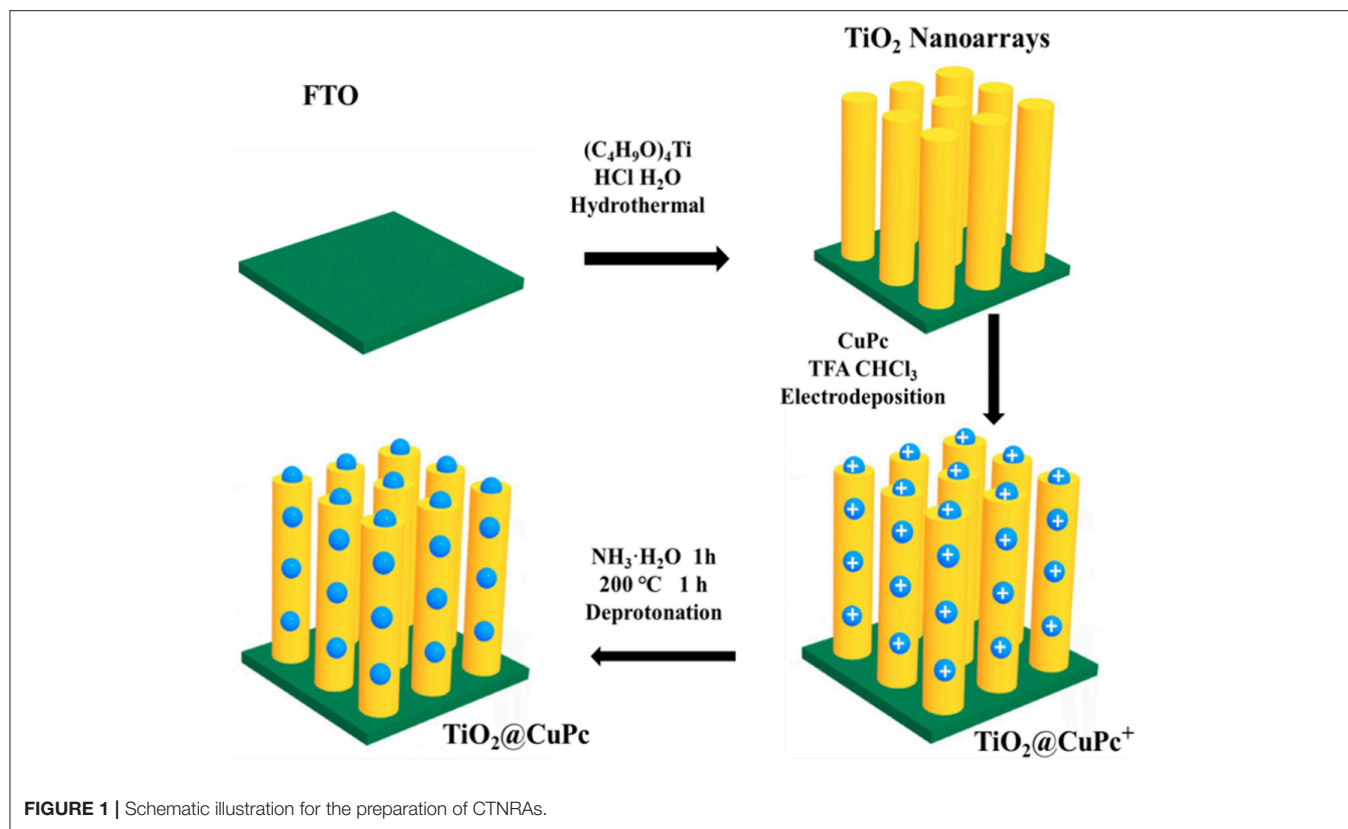
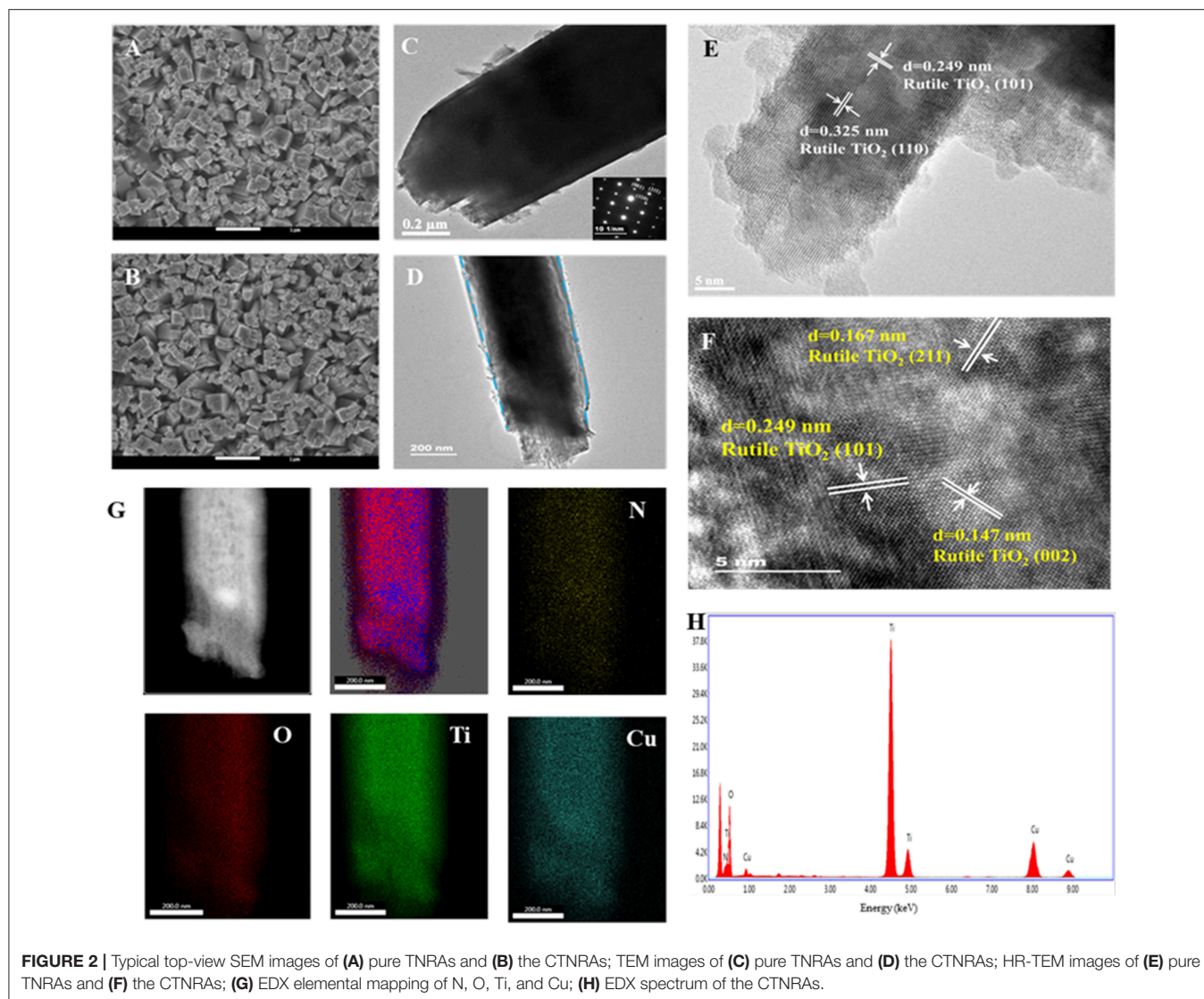


**FIGURE 1** | Schematic illustration for the preparation of CTNRAs.

of rutile TiO<sub>2</sub>. In contrast, the characteristic Raman peaks located at 1,535, 1,338, and 685 cm<sup>-1</sup> are observed in the CuPc samples (Ludemann et al., 2011), which could be accordance with the C-N stretching vibration on pyrrole bonded to central copper ion, C-N stretching vibration peak on heterocyclic ring and vibration of large phthalocyanine ring, respectively. As for the sample of CTNRAs all characteristic peaks of CuPc and rutile TiO<sub>2</sub> could be seen with a slightly shift, which further elucidate the existence of CuPc on CTNRAs. Optical properties of CTNRAs, CuPc, and TNRAs were measured by UV-Vis absorption measurement (Figures S6, S7). Owing to the broad band gap (3.0 eV), TiO<sub>2</sub> only reveal a strong absorption at wavelength shorter than 410 nm. CuPc display strong absorption bands in the range of 500–800 nm. In comparison, TiO<sub>2</sub>@CuPc sample exhibit a strong absorption shorter than 410 nm, and two very weak absorption peaks at about 550 and 650 nm which results from CuPc due to the lower deposition amount.

In order to further confirm the existence of CuPc in TNRAs and understand the surface chemical state of the sample, we have employed the X-ray photoelectron spectroscopy (XPS) measurements. Obvious photoelectron peaks of C, N, Cu, O, and Ti elements are observed in the XPS survey spectrum (Figure 3C) of CTNRAs. In compare with pristine TNRAs, TCNRAs contain not only Ti, O and C elements from TNRAs, but also Cu and N elements from CuPc. The high resolution Ti 2p XPS spectrum (Figure 3D) shows two different peaks at 462.4 eV and 458.4 eV, which can be ascribed to the characteristic of Ti 2p<sub>1/2</sub> and Ti 2p<sub>2/3</sub> deriving from Ti<sup>4+</sup>, respectively. Furthermore, the O 1s spectra (Figure S8) of TNRAs and CTNRAs can be factored into

two peaks at about 529.6 and 530.1 eV. The peak 1 at about 530.1 eV is ascribed to surface Ti-OH species, while peak 2 is assigned to lattice oxygen in O-Ti<sup>4+</sup>. Compared to pure TiO<sub>2</sub>, the deposition of CuPc reduces the area ratio of peak 1 to peak 2, maybe indicating the surface of TiO<sub>2</sub> was covered by CuPc, so that it adsorb less amount of OH groups. It can be seen from Figure 3E that the high resolution XPS spectrum of Cu 2p in CTNRAs has two strong peaks at 954.3 and 934.5 eV, which are the Cu 2p<sub>1/2</sub> and Cu 2p<sub>2/3</sub>, respectively. The binding energy of the Cu 2p<sub>2/3</sub> is 934.5 eV, indicating that the Cu atom in the CTNRAs exists in the Cu (II) state (Zheng et al., 2004). This data can be explained by the chemical structure of the CuPc molecule, in which the copper exists in the bivalent form. In addition, the satellite peak of the Cu(II) state can be seen, which imply that the CuPc molecular plane contains 3dx<sup>2</sup>-y<sup>2</sup> orbitals. From the fine spectrum of N 1s (Figure 3F), we can see two peaks located at 400.1 eV and 398.6 eV. N atoms have two chemical environments in CuPc, one is C-N=C bond forming by 4 C atoms with 2 N atoms which located in 398.6 eV, the other is the 4 N atoms coordination bonding with the Cu atom, the signal of which located at 400.1 eV. As for high resolution XPS spectrum of C 1s (Figure S9), there are two types of carbon atoms in the CTNRAs 8 C atoms are bonded to 2 N atoms forming N-C=N bond at 289.4 eV; the remaining 24 C atoms have aromatic hydrocarbon properties which is located at 285.0 eV. With decided contrast, the XPS spectrum of pure TNRAs only have a C 1S signal at 284.8 eV, which can be attributed to the absorbed contaminants. Combined with the results of XRD analysis, Raman spectra and UV-Vis absorption, we concluded that CuPc indeed assembled



onto the surface of TNRAs to form a uniform coverage through electro-induced assembly. As far as the assembled pattern of CuPc on the surface of TiO<sub>2</sub> nanorod was concerned, we inferred that the plane CuPc molecules adopt a flattened pattern rather than a standing pattern on the surface of TiO<sub>2</sub> nanorod through electrostatic self-assembly because CuPc have a plane structure and the positive charge located near the center of the plane, so the flattened pattern is more stable than the standing pattern, which will be proved by the good stability of obtained device for PEC operation.

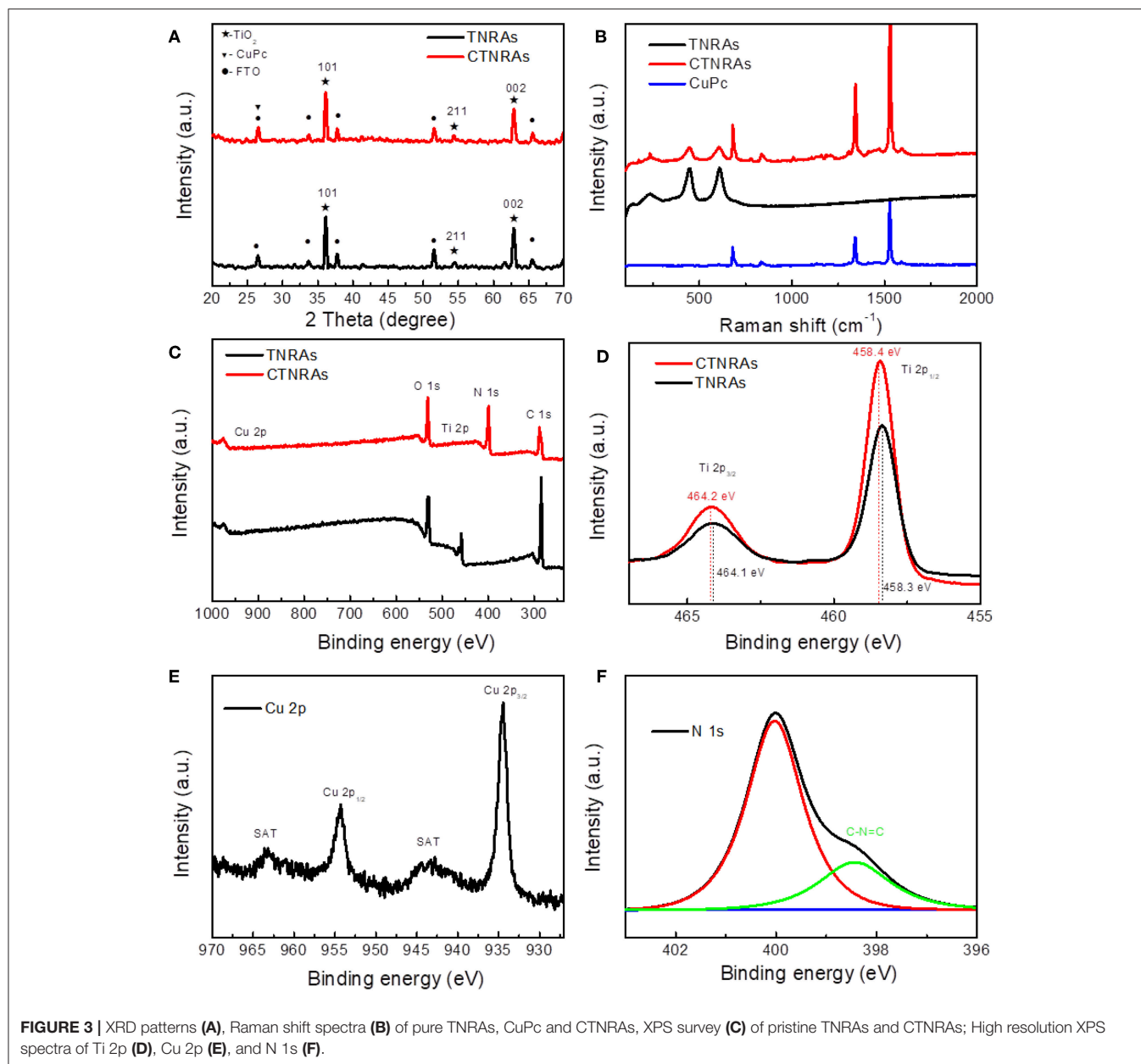
The linear sweep voltammetry (LSV) curves showed in **Figure 4A** reveals the photoelectrochemical (PEC) activities of the as-prepared samples. Under 100 mW/cm<sup>2</sup> irradiation by the simulated solar light (AM 1.5G), transient photocurrent responses of pristine TNRAs is 1.01 mA/cm<sup>2</sup> at 1.23 V (vs. RHE), while pure CuPc almost have no PEC response. After coating with CuPc, the photocurrent density of CTNRAs showed dramatically increase. With the electrodeposition time

prolonged, the photocurrent density increased first and then decreased (**Figure S15**). The optimized electrodeposition time is 60 s, the photocurrent density reaches 2.40 mA/cm<sup>2</sup> at 1.23 V (vs. RHE), which was 2.40 times as that of pure TNRAs. Then, the photocurrent response was decrease when electrodeposition time longer than 60 s. The photocurrent density of CTNRAs was 1.80, 1.60, and 1.30 mA/cm<sup>2</sup>, when the electrodeposition time was 90, 120, and 150 s, respectively.

To more intuitive observe the relationship between the photocurrent density enhancement and the deposition time of the CTNRAs, the curve of growth rate of photocurrent density vs. deposition time was plotted in **Figure 4B**. Growth rate can be expressed concretely as:

$$\text{Growth ratio} = \frac{I_{\text{CTNRAs}} - I_{\text{TNRAs}}}{I_{\text{TNRAs}}} \times 100\%$$

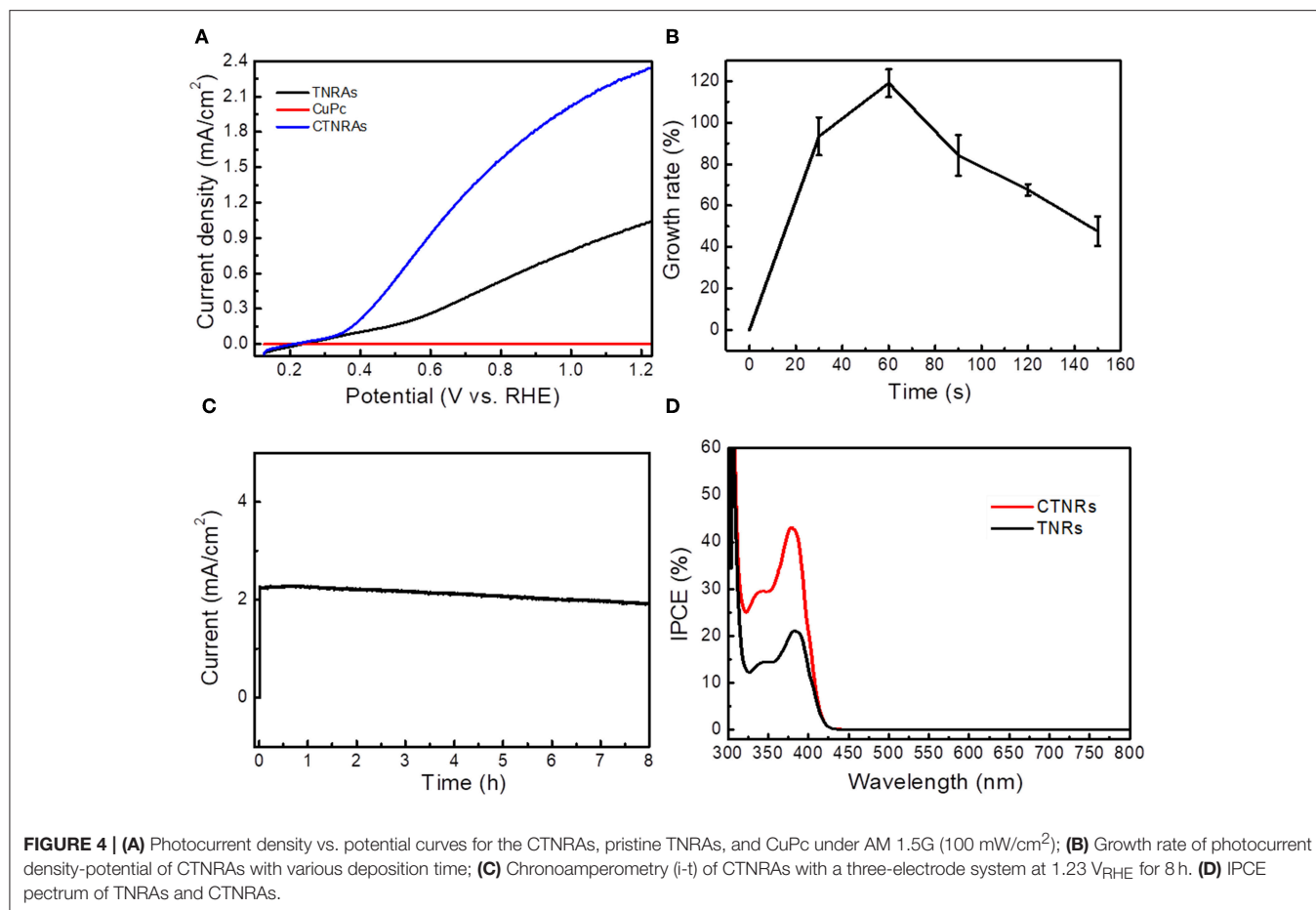
Where  $I_{\text{CTNRAs}}$  and  $I_{\text{TNRAs}}$  were the photocurrent density of CTNRAs and TNRAs, respectively. The plot was shown as a



single peak curve that the growth ratio increased rapidly as the deposition time <60 s and reaches the maximum average growth rate of about 120% at 60 s. When the time was prolonged further, the growth ratio declined with deposition time. ICP-MS measurements was carried out to estimate the loaded amount of CuPc on the surface of TNRAs, when the electrodeposition time was 30, 60, 90, 120, and 150 s, the anchoring mass of CuPc was 0.024, 0.047, 0.069, 0.089, and 0.112  $\mu\text{mol}$  on per square centimeter TiO<sub>2</sub>, respectively. With the amount of CuPc increased, the photocurrent density increased first and then decreased. And the fine XPS spectrum of Cu<sub>2p</sub> and Ti<sub>2p</sub> in the optimized CTNRAs sample was calculated carefully to estimate the surface atom ratio of Ti and Cu (Figure S10), the results

illustrated that the surface atom ratio of Ti and Cu from the optimized sample was about 30:1.

The stability of the optimized CTNRAs was detected by photocurrent-time (I-t) measurement at 1.23 V vs. RHE under continuous illumination (100 mW/cm<sup>2</sup>, AM 1.5G) for 8 h (Figure 4C). Starting without illumination, the photocurrent density is almost zero. When illumination was opened, the photocurrent density reached 2.40 mA/cm<sup>2</sup>. The value of photocurrent density stays almost no decline in the long 8 h operation which means that CTNRAs have a good stability for PEC water oxidation. To observe the composition and morphology change of the device during the process of PEC operation, SEM, XPS and ICP-MS measurements were



conducted. The results shown that: (1) the morphology of the electrode after operation is almost the same as that before operation (**Figure S5**); (2) XPS measurement (**Figures S11, S12**) confirmed the exist of CuPc on the sample after operation, but the ICP measurement show that the loaden amount of CuPc is declined compared to the sample before operation. This is probably due to the slight leakage of CuPC during the PEC process.

Incident photon-to-current conversion efficiency (IPCE) was measured at 1.23 V vs. RHE, to further elucidate the enhanced PEC oxygen production performance of CTNRAs. IPCE (Cho et al., 2011) can be calculate concretely as:

$$\text{IPCE} = \frac{(1240 \times J)}{(\lambda \times I)} \times 100\%$$

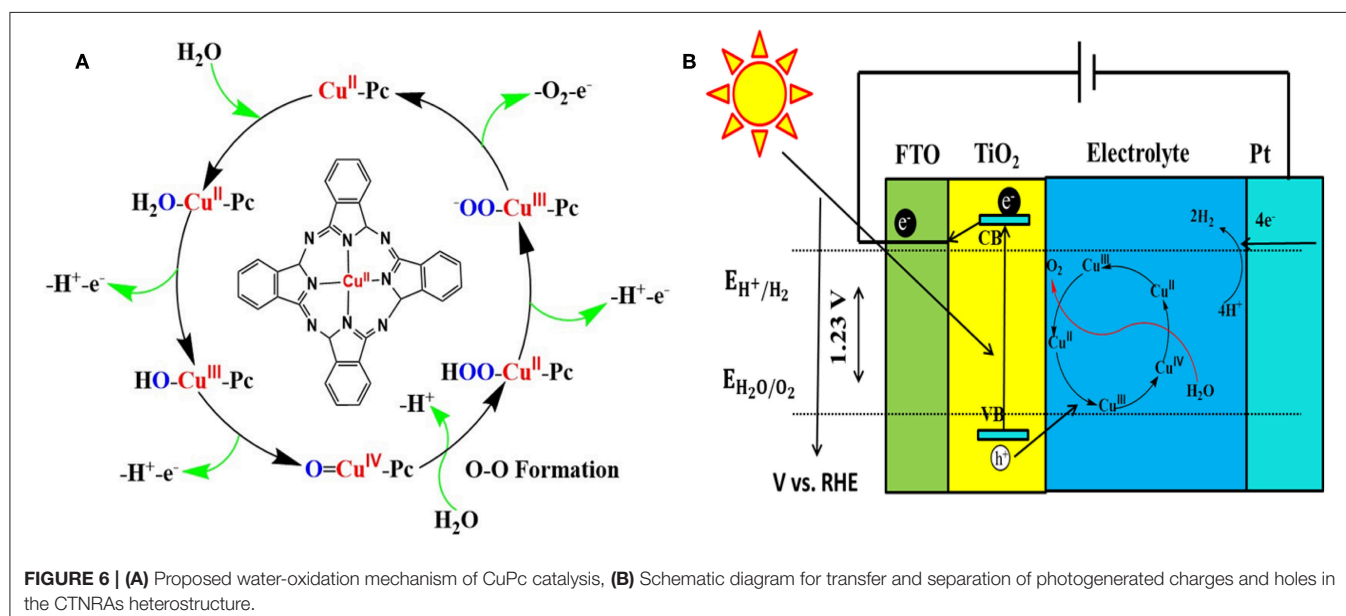
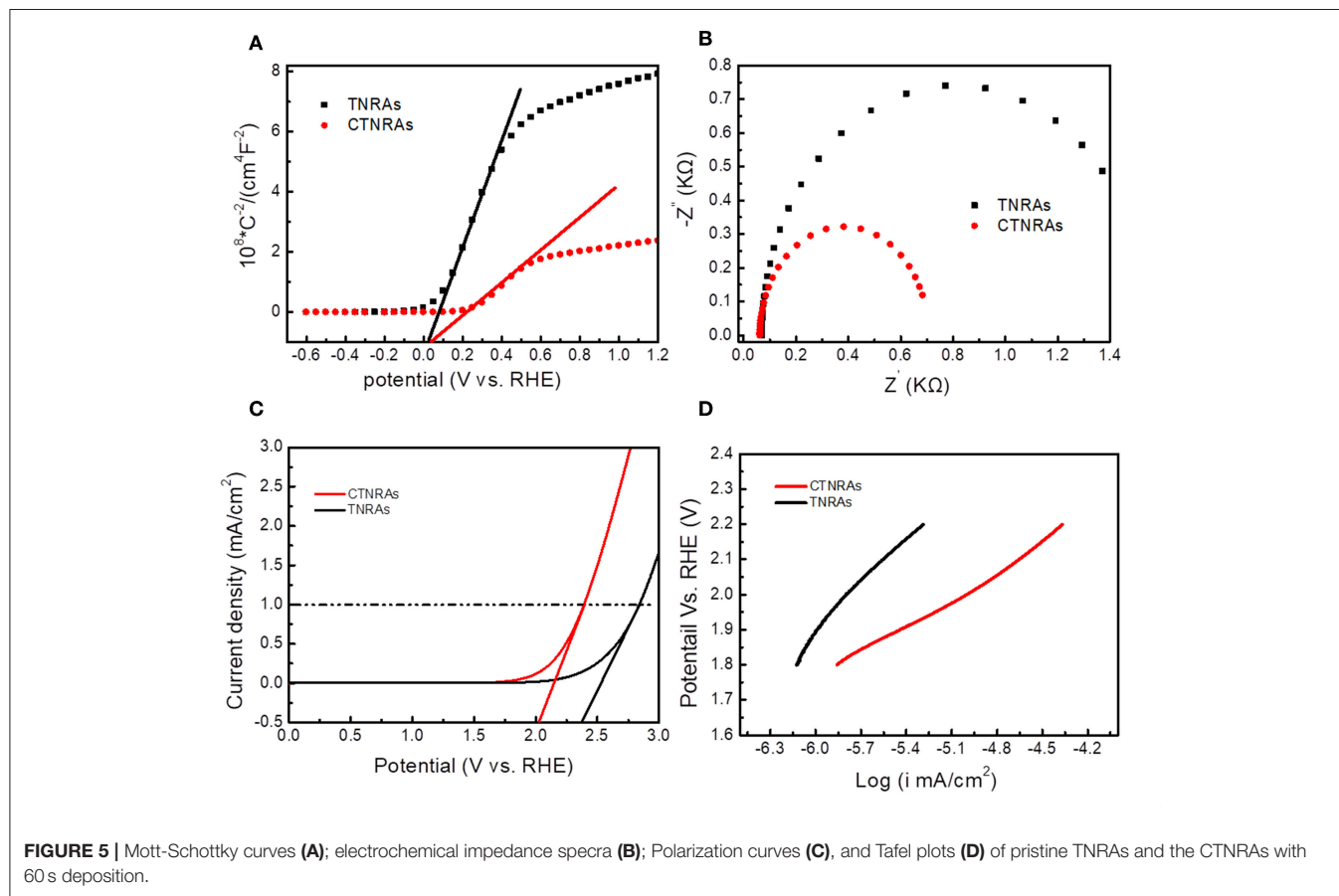
Where  $\lambda$  and  $I$  are the incident light wavelength and the power density for each wavelength, respectively, and  $J$  is the photocurrent density produced by excited electrons. As shown in **Figure 4D**, the IPCE of CTNRAs is higher than that of pristine TNRAs in the whole spectrum, which indicates that the photogenerated electron-hole pairs are effectively separated in the CTNRAs. The IPCE value was reached 45% at 380 nm, but the IPCE of pure TNRAs is only 21%. The IPCE value

can be improved by enhancing the charge injection efficiency, efficiency of light capture and charge collection efficiency. CTNRAs not only have TiO<sub>2</sub> nanorod arrays that are grown perpendicularly to the FTO substrate with a large surface area, in case to enhance the light harvesting efficiency, but also have CuPc layer which can provide a direct pathway for excited holes to improve the collection efficiency and water oxidation kinetics. Accordingly, the IPCE of CTNRAs can reach as high as 45%.

In order to further verify the proposed mechanism, Mott-Schottky measurements were used to obtain flat band potential and the charge carrier density of the interface between semiconductors. The positive slope of CTNRAs and pristine TNRAs (**Figure 5A**) suggests the expected n-type semiconductor of TiO<sub>2</sub> in the nanocomposites. For n-type semiconductor, flat band potential is consistent with the bottom of the conduction band. Pristine TNRAs and CTNRAs have the same flat band voltage, implying that the deposition of CuPc did not change the flat band position of TNRAs. From the results of Mott-Schottky measurements, we excluded the possibility of p-n junction formation between the interface of CuPc and TNRAs, which also confirmed by the IPCE measurements where no response was observed from the longer wavelength according to the absorption of CuPc.

In order to further understand the enhanced PEC performance, the inherent electronic properties of CTNRAs were characterized by measuring electrochemical impedance spectroscopy (EIS), the onset OER potential and linear Tafel

plots. It is well-known that the larger over potential of TNRAs for water oxidation, presenting the sluggish kinetics, which can limit its wide application in PEC water splitting. The onset potential for OER of TNRAs and CTNRAs (**Figure 5C**) is 2.36,



and 2.04 V, respectively, which indicate electrocatalytic activity in CTNRAs was greatly enhanced by the deposition of CuPc. Electrochemical impedance is an effective method for assessing the kinetic of electron transfer at the electrode-electrolyte interface. From **Figure 5B**, electrochemical impedance spectra show that pristine TNRAs has higher resistance than CTNRAs, indicating the loading of CuPc effectively promote the separation of electron and hole and enable high-speed electron transport for water splitting.

The Tafel plot depicts the relationship between the logarithm of the current density ( $i_k$ ) and the over potential ( $\eta$ ), which is an important parameter for water splitting electrocatalysts and can provide important information about electronic enhancement of electrocatalysts activity (Tong et al., 2014). Generally, the decrease in the slope of the curve represents an increased kinetics for PEC oxygen revolution. As shown in **Figure 5D**, the slope of the Tafel curve for TNRAs and CTNRAs is about 405, and 256 mV per decade, respectively. The result show CTNRAs has lower slope value than TNRAs, which can indicate TNRAs has a more sluggish kinetics than CTNRAs.

To validate the mechanism of PEC performance enhancement by CuPc deposition, we compared the cyclic voltamm spectra of TNRAs and CTNRAs, there exist two unobvious oxidation peaks located at about 1.3 and 1.8 V vs. RHE in the CV curve of CTNRAs, while there are not any oxidation peaks in the same range in the CV curve of TNRAs (**Figure S13**). Then the LSV curve of CuPc deposited on FTO with that of blank FTO, as shown in **Figure S14A**, the onset potential of CuPc is about 2.01 V vs. RHE, while the onset potential of blank FTO anode is about 2.29 V vs. RHE under the same conditions. Obvious cathodic shift of onset potential about 280 mV is observed, indicating that CuPc has acted as a co-catalyst for electrochemical water oxidation which is coincident with the results of Mott-Schottky. In order to further clarify the detailed process of water oxidation catalyzed by CuPc, the cycle voltammetry (CV) curves were measured and the results was shown in **Figure S14B**. Compared with the CV curve of blank FTO, there appeared two more oxidation peaks located at 1.31 and 1.69 V vs. RHE in the CV curve of CuPc, which could be attributed to the oxidation process of  $\text{Cu}^{2+}$  to  $\text{Cu}^{3+}$  and  $\text{Cu}^{3+}$  to  $\text{Cu}^{4+}$ , respectively (Zhang et al., 2013). Based on the electrochemical analysis above, a possible mechanism for water-oxidation catalyzed by CuPc was proposed (**Figure 6A**). During the PEC process, a water molecule from solution firstly coordinated to Cu center of CuPc molecule anchored on the surface of the electrode to form hydrated copper phthalocyanine (Li et al., 2012). As follows, the resulting  $\text{H}_2\text{O}=\text{Cu}^{\text{II}}\text{-Pc}$  is oxidized through a PCET to yield a  $\text{HO}=\text{Cu}^{\text{III}}\text{-Pc}$ , which can be further oxidized to a  $\text{O}=\text{Cu}^{\text{IV}}\text{-Pc}$  by PCET. Next,  $\text{O}=\text{Cu}^{\text{IV}}\text{-Pc}$  is attacked by  $\text{H}_2\text{O}$  or  $\text{OH}^-$  from the electrolyte, correspondingly, and O-O bond can be generated. The process is in accordance with the water nucleophilic attack (WNA) mechanism.  $\text{HOO}-\text{Cu}^{\text{II}}\text{-Pc}$  is an important intermediate in the peroxide bridge structure, which can be further oxidized to a  $^-\text{OO}=\text{Cu}^{\text{IV}}\text{-Pc}$  by PCET, then releases oxygen molecules and the CuPc species restore to the initial state.

Based on the characterizations as mentioned earlier, a possible mechanism for the PEC performance improvement over CTNRAs is proposed as shown in **Figure 6B**. Under simulated sunlight irradiation, photo generated electrons are excited from the valence band (VB) of  $\text{TiO}_2$  to its conduction band (CB), leaving holes in VB of  $\text{TiO}_2$ . Ultimately, electrons pass through the external circuit to the counter electrode and  $\text{H}^+$  were reduced to produce  $\text{H}_2$ . Accordingly, the holes from VB of  $\text{TiO}_2$  were consumed by the process in which  $\text{Cu}^{2+}$  is oxidized to  $\text{Cu}^{3+}$  and then to  $\text{Cu}^{4+}$ . In the process of water oxidation, the presence of CuPc derived species is considered to be a fast redox mediator, which not only reduce the activation energy of PEC water oxidation, but promote effective charge separation as well.

## CONCLUSION

In conclusion, through a simple electro-induced assembly method  $\pi$ -conjugated copper phthalocyanine was successfully deposited on the surface of  $\text{TiO}_2$  nanorod arrays to form organic-inorganic hybrid nanostructures which were directly grown on the FTO substrate. The obtained hybrid nanostructures can be used as photoanode for PEC water splitting with enhanced performance and good stability. Electrodeposited copper phthalocyanine molecules were proved to act as a co-catalyst for PEC water oxidation rather than a p-type semiconductor to form p-n junction with  $\text{TiO}_2$ . Detailed mechanism was also proposed based on detailed experiments and analysis. This design establishes a cost-effective surficial assembly strategy to fabricate PEC device with enhanced performance using functional  $\pi$ -conjugated molecules in the field of PEC water splitting, carbon dioxide reduction and other related energy-storing reactions.

## AUTHOR CONTRIBUTIONS

YL designed experiments. MY carried out experiments. ZT, NL, and HZ analyzed experimental results. YaL, AZ, and SX analyzed sequencing data and gave helpful discussions to the conclusions. MY and YL wrote the manuscript.

## ACKNOWLEDGMENTS

We thank the National Natural Science Foundation of China (21103134, 21675124) and the financial support from Beijing National Laboratory for Molecular Sciences (BNLMS201825) and the ACS key lab of Colloids, interfaces, and Thermal Dynamics. We also thank Prof. Kaiqiang Liu and Mr. Xiangyang Yan (School of Chemistry and Chemical Engineering, Shaanxi Normal University) for their technical supports in TEM and XPS measurements.

## SUPPLEMENTARY MATERIAL

The Supplementary Material for this article can be found online at: <https://www.frontiersin.org/articles/10.3389/fchem.2019.00334/full#supplementary-material>

## REFERENCES

- Akira, F., and Kenichi, H. (1972). Electrochemical photolysis of water at a semiconductor electrode. *Nature* 238, 37–38. doi: 10.1038/238037a0
- Artero, V., Chavarot-Kerlidou, M., and Fontecave, M. (2011). Splitting water with cobalt. *Angew. Chem. Int. Ed. Engl.* 50, 7238–7266. doi: 10.1002/anie.201007987
- Bessel, K., Borbush, F., and McGloin, M. (2010). Cooperation of charges in photosynthetic O<sub>2</sub> evolution-I. A linear four step mechanism. *Photochem. Photobiol.* 11, 457–475. doi: 10.1111/j.1751-1097.1970.tb06017.x
- Bin, L., and Aydil, E. S. (2009). Growth of oriented single-crystalline rutile TiO<sub>2</sub> nanorods on transparent conducting substrates for dye-sensitized solar cells. *J. Am. Chem. Soc.* 131, 3985–3990. doi: 10.1021/ja8078972
- Blakemore, J. D., Schley, N. D., David, B., Hull, J. F., Olack, G. W., Incarvito, C. D., et al. (2010). Half-sandwich iridium complexes for homogeneous water-oxidation catalysis. *J. Am. Chem. Soc.* 132, 16017–16029. doi: 10.1021/ja104775j
- Chauhan, M., Reddy, K. P., Gopinath, C. S., and Deka, S. (2017). Copper cobalt sulphide nanosheets realizing promising electrocatalytic oxygen evolution reaction. *ACS Catal.* 7, 5871–5879. doi: 10.1021/acscatal.7b01831
- Chen, P., Chen, Z., and Liu, M. (2008). Nanotapes formed through the air/water interfacial self-assembly of a bola-form pentanediamide derivative. *Colloid. Surface. A* 313, 666–669. doi: 10.1016/j.colsurfa.2007.04.142
- Cherevko, S., Geiger, S., Kasian, O., Kulyk, N., Grote, J. P., Sazan, A., et al. (2015). Oxygen and hydrogen evolution reactions on Ru, RuO<sub>2</sub>, Ir, and IrO<sub>2</sub> thin film electrodes in acidic and alkaline electrolytes: a comparative study on activity and stability. *Catal. Today* 262, 170–180. doi: 10.1016/j.cattod.2015.08.014
- Cho, I. S., Chen, Z., Forman, A. J., Kim, D. R., Rao, P. M., Jaramillo, T. F., et al. (2011). Branched TiO<sub>2</sub> nanorods for photoelectrochemical hydrogen production. *Nano Lett.* 11, 4978–4984. doi: 10.1021/nl2029392
- Ding, C., Shi, J., Wang, Z., and Li, C. (2017). Photoelectrocatalytic water splitting: significance of cocatalysts, electrolyte and interfaces. *ACS Catal.* 7, 675–688. doi: 10.1021/acscatal.6b03107
- Du, J., Zhou, G., Zhang, H., Cheng, C., Ma, J., Wei, W., et al. (2013). Ultrathin porous NiCo<sub>2</sub>O<sub>4</sub> nanosheet arrays on flexible carbon fabric for high-performance supercapacitors. *ACS Appl. Mater. Inter.* 5, 7405–7409. doi: 10.1021/am4017335
- Du, P., and Eisenberg, R. (2012). Catalysts made of earth-abundant elements (Co, Ni, Fe) for water splitting: recent progress and future challenges. *Energy Environ. Sci.* 5, 6012–6021. doi: 10.1039/c2ee03250c
- Fang, M., Dong, G., Wei, R., and Ho, J. C. (2017). Hierarchical nanostructures: design for sustainable water splitting. *Adv. Energy Mater.* 7:1700559. doi: 10.1002/aenm.201700559
- Ferreira, K. N., Iverson, T. M., Maghlaoui, K., Barber, J., and Iwata, S. (2004). Architecture of the photosynthetic oxygen-evolving center. *Science* 303, 1831–1838. doi: 10.1126/science.1093087
- Geng, G., Wang, Z., Chen, P., Guan, B., Yang, C., and Liu, M. (2018). Platinized spherical supramolecular nanoassemblies of a porphyrin: facile synthesis and excellent catalytic recyclability. *Phys. Chem. Chem. Phys.* 20, 8488–8497. doi: 10.1039/c8cp00173a
- Gibson, L., Wilman, E. N., and Lurance, W. F. (2017). How green is 'green' energy? *Trends. Ecol. Evol.* 32, 922–935. doi: 10.1016/j.tree.2017.09.007
- Gong, Y. N., Ouyang, T., He, C. T., and Lu, T. B. (2016). Photoinduced water oxidation by an organic ligand incorporated into the framework of a stable metal-organic framework. *Chem. Sci.* 7, 1070–1075. doi: 10.1039/c5sc02679b
- Guo, P., Chen, P., and Liu, M. (2011). Shuttle-like supramolecular nanostructures formed by self-assembly of a porphyrin via an oil/water system. *Nanoscale Res. Lett.* 6, 529–538. doi: 10.1186/1556-276X-6-529
- Guo, P., Chen, P., Ma, W., and Liu, M. (2012). Morphology-dependent supramolecular photocatalytic performance of porphyrin nanoassemblies: from molecule to artificial supramolecular nanoantenna. *J. Mater. Chem.* 22, 20243–20249. doi: 10.1039/c2jm33253a
- Hang, M. H., Mao, S., Feick, H., Yan, H., Wu, Y., Kind, H., et al. (2001). Room-temperature ultraviolet nanowire nanolasers. *Cheminform* 32, 1897–1899. doi: 10.1126/science.1060367
- Haumann, M., Liebisch, P., Muller, C., Barra, M., Grabolle, M., and Dau, H. (2005). Photosynthetic O<sub>2</sub> formation tracked by time-resolved x-ray experiments. *Science* 310, 1019–1021. doi: 10.1126/science.1117551
- Jeong, K., Deshmukh, P. R., Park, J., Sohn, Y., and Shin, W. G. (2018). ZnO-TiO<sub>2</sub> core-shell nanowires: a sustainable photoanode for enhanced photoelectrochemical water splitting. *ACS Sustain. Chem. Eng.* 6, 6518–6526. doi: 10.1021/acssuschemeng.8b00324
- Jiang, X., Yu, Z., Lai, J., Zhang, Y., Lei, N., Wang, D., et al. (2017). Efficient perovskite solar cells employing a solution-processable copper phthalocyanine as a hole-transporting material. *Sci. China Chem.* 60, 119–126. doi: 10.1007/s11426-016-0393-5
- Junya, S., Nobuo, S., Yoko, Y., Kazuhiko, M., Tsuyoshi, T., Kondo, J. N., et al. (2005). RuO<sub>2</sub>-loaded beta-Ge<sub>3</sub>N<sub>4</sub> as a non-oxide photocatalyst for overall water splitting. *J. Am. Chem. Soc.* 127, 4150–4151. doi: 10.1021/ja042973v
- Kumar, D. P., Reddy, N. L., Srinivas, B., Durgakumari, V., Roddatis, V., Bondarchuk, O., et al. (2016). Stable and active Cu<sub>x</sub>O/TiO<sub>2</sub> nanostructured catalyst for proficient hydrogen production under solar light irradiation. *Sol. Energ. Mat. Sol. C* 146, 63–71. doi: 10.1016/j.solmat.2015.11.030
- Lauinger, S. M., Sumliner, J. M., Yin, Q., Xu, Z., Liang, G., Glass, E. N., et al. (2015). High stability of immobilized polyoxometalates on TiO<sub>2</sub> nanoparticles and nanoporous films for robust, light-induced water oxidation. *Chem. Mater.* 27, 5886–5891. doi: 10.1021/acs.chemmater.5b01248
- Lee, P. S., and Chen, X. (2014). Nanomaterials for energy and water management. *Small* 10, 3432–3433. doi: 10.1002/sml.201402027
- Li, B., Li, F., Bai, S., Wang, Z., Sun, L., Yang, Q., et al. (2012). Oxygen evolution from water oxidation on molecular catalysts confined in the nanocages of mesoporous silicas. *Energy Environ. Sci.* 5, 8229–8233. doi: 10.1039/c2ee22059h
- Li, H., Gao, Y., Zhou, Y., Fan, F., Han, Q., Xu, Q., et al. (2016a). Construction and nanoscale detection of interfacial charge transfer of elegant Z-scheme WO<sub>3</sub>/Au/In<sub>2</sub>S<sub>3</sub> nanowire arrays. *Nano Lett.* 16, 5547–5552. doi: 10.1021/acs.nanolett.6b02094
- Li, Q., Liu, Y., Guo, S., and Zhou, H. (2017). Solar energy storage in the rechargeable batteries. *Nano Today* 16, 46–60. doi: 10.1016/j.nantod.2017.08.007
- Li, Y., Feng, J., Li, H., Wei, X., Wang, R., and Zhou, A. (2016b). Photoelectrochemical splitting of natural seawater with Fe<sub>2</sub>O<sub>3</sub>/WO<sub>3</sub> nanorod arrays. *Int. J. Hydrogen Energy* 41, 4096–4105. doi: 10.1016/j.ijhydene.2016.01.027
- Li, Y., Wang, R., Li, H., Wei, X., Feng, J., Liu, K., et al. (2015). Efficient and stable photoelectrochemical seawater splitting with TiO<sub>2</sub>@g-C<sub>3</sub>N<sub>4</sub> nanorod arrays decorated by Co-Pi. *J. Phys. Chem. C* 119, 20283–20292. doi: 10.1021/acs.jpcc.5b05427
- Li, Y., Wei, X., Zhu, B., Wang, H., Tang, Y., Sum, T. C., et al. (2016c). Hierarchically branched Fe<sub>2</sub>O<sub>3</sub>@TiO<sub>2</sub> nanorod arrays for photoelectrochemical water splitting: facile synthesis and enhanced photoelectrochemical performance. *Nanoscale* 8, 11284–11290. doi: 10.1039/c6nr02430k
- Liu, B., Wang, D., Wang, L., Sun, Y., Lin, Y., Zhang, X., et al. (2013). Glutathione-assisted hydrothermal synthesis of CdS-decorated TiO<sub>2</sub> nanorod arrays for quantum dot-sensitized solar cells. *Electrochim. Acta* 113, 661–667. doi: 10.1016/j.electacta.2013.09.143
- Liu, L., Ji, Z., Zou, W., Gu, X., Deng, Y., Gao, F., et al. (2013). *In situ* loading transition metal oxide clusters on TiO<sub>2</sub> nanosheets as co-catalysts for exceptional high photoactivity. *ACS Catal.* 3, 2052–2061. doi: 10.1021/cs4002755
- Liu, M., Zhang, L., and Wang, T. (2015). supramolecular chirality in self-assembled systems. *Chem. Rev.* 115, 7304–7397. doi: 10.1021/cr500671p
- Long, C., Li, X., Guo, J., Shi, Y., Liu, S., and Tang, Z. (2018). Electrochemical reduction of CO<sub>2</sub> over heterogeneous catalysts in aqueous solution: recent progress and perspectives. *Small Method.* 2018:1800369. doi: 10.1002/smt.201800369
- Lu, C., Du, J., Su, X. J., Zhang, M. T., Xu, X., Meyer, T. J., et al. (2016). Cu(II) aliphatic diamine complexes for both heterogeneous and homogeneous water oxidation catalysis in basic and neutral solutions. *ACS Catal.* 6, 77–83. doi: 10.1021/acscatal.5b02173
- Ludemann, M., Brumboiu, I. E., Gordan, O. D., and Zahn, D. R. T. (2011). Surface-enhanced Raman effect in ultra-thin CuPc films employing periodic silver nanostructures. *J. Nanopart. Res.* 13, 5855–5861. doi: 10.1007/s11051-011-0564-z
- Meyer, T. J., Sheridan, M. V., and Sherman, B. D. (2017). Mechanisms of molecular water oxidation in solution and on oxide surfaces. *Chem. Soc. Rev.* 46, 6148–6169. doi: 10.1039/c7cs00465f

- Nepal, B., and Das, S. (2013). Sustained water oxidation by a catalyst cage-isolated in a metal-organic framework. *Angew. Chem. Int. Ed. Engl.* 52, 7224–7227. doi: 10.1002/anie.201301327
- Ogunsipe, A., and Nyokong, T. (2004). Effects of substituents and solvents on the photochemical properties of zinc phthalocyanine complexes and their protonated derivatives. *J. Mol. Struct. J. Mol. Struct.* 689, 89–97. doi: 10.1016/j.molstruc.2003.10.024
- Osterloh, F. E. (2013). Inorganic nanostructures for photoelectrochemical and photocatalytic water splitting. *Chem. Soc. Rev.* 42, 2294–2320. doi: 10.1039/c2cs35266d
- Qiu, Y., Chen, P., and Liu, M. (2010). Evolution of various porphyrin nanostructures via an oil/aqueous medium: controlled self-assembly, further organization, and supramolecular chirality. *J. Am. Chem. Soc.* 132, 9644–9652. doi: 10.1021/ja1001967
- Ran, J., Zhang, J., Yu, J., Jaroniec, M., and Qiao, S. Z. (2014). Earth-abundant cocatalysts for semiconductor-based photocatalytic water splitting. *Chem. Soc. Rev.* 43, 7787–7812. doi: 10.1039/c3cs60425j
- Seh, Z. W., Kibsgaard, J., Dickens, C. F., Chorkendorff, I., Nørskov, J. K., and Jaramillo, T. F. (2017). Combining theory and experiment in electrocatalysis: insights into materials design. *Science* 355, 4998–5013. doi: 10.1126/science.aad4998
- Shi, T., Duan, Y., Lv, K., Hu, Z., Li, Q., Li, M., et al. (2018). Photocatalytic oxidation of acetone over high thermally stable TiO<sub>2</sub> nanosheets with exposed (001) facets. *Front. Chem.* 6:175. doi: 10.3389/fchem.2018.00175
- Su, J., Xue, M., Ma, N., Sheng, Q., Zhang, Q., and Liu, Y. (2009). Dissolution of copper phthalocyanine and fabrication of its nano-structure film. *Sci. China Ser. B* 52, 911–915. doi: 10.1007/s11426-009-0021-3
- Su, X. J., Gao, M., Jiao, L., Liao, R. Z., Siegbahn, P. E., Cheng, J. P., et al. (2015). Electrocatalytic water oxidation by a dinuclear copper complex in a neutral aqueous solution. *Angew. Chem. Int. Ed. Engl.* 54, 4909–4914. doi: 10.1002/anie.201411625
- Tang, R., Zhou, S., Yuan, Z., and Yin, L. (2017). Metal-organic framework derived Co<sub>3</sub>O<sub>4</sub>/TiO<sub>2</sub> /Si heterostructured nanorod array photoanodes for efficient photoelectrochemical water oxidation. *Adv. Funct. Mater.* 27:1701102. doi: 10.1002/adfm.201701102
- Terao, R., Nakazono, T., Parent, A. R., and Sakai, K. (2016). Photochemical water oxidation catalysed by a water-soluble copper phthalocyanine. *Chempluschem* 81, 1064–1067. doi: 10.1002/cplu.201600263
- Tong, X., Yang, P., Wang, Y., Qin, Y., and Guo, X. (2014). Enhanced photoelectrochemical water splitting performance of TiO<sub>2</sub> nanotube arrays coated with an ultrathin nitrogen-doped carbon film by molecular layer deposition. *Nanoscale* 6, 6692–6700. doi: 10.1039/c4nr00602j
- Wang, H., Bai, Y., Wu, Q., Zhou, W., Zhang, H., Li, J., et al. (2011). Rutile TiO<sub>2</sub> nano-branched arrays on FTO for dye-sensitized solar cells. *Phys. Chem. Chem. Phys.* 13, 7008–7013. doi: 10.1039/c1cp20351g
- Wang, H., Yang, Y., and Guo, L. (2016). Nature-inspired electrochemical energy-storage materials and devices. *Adv. Energy Mater.* 7:1601709. doi: 10.1002/aenm.201601709
- Wang, X., Duan, P., and Liu, M. (2014). Self-assembly of pi-conjugated gelators into emissive chiral nanotubes: emission enhancement and chiral detection. *Chem. Asian. J.* 9, 770–778. doi: 10.1002/asia.201301518
- Xiao, F. X., Miao, J., Tao, H. B., Hung, S. F., Wang, H. Y., Yang, H. B., et al. (2015). One-dimensional hybrid nanostructures for heterogeneous photocatalysis and photoelectrocatalysis. *Small* 11, 2115–2131. doi: 10.1002/smll.201402420
- Yang, J., Li, W., Li, J., Sun, D., and Chen, Q. (2012). Hydrothermal synthesis and photoelectrochemical properties of vertically aligned tungsten trioxide (hydrate) plate-like arrays fabricated directly on FTO substrates. *J. Mater. Chem.* 22, 17744–17752. doi: 10.1039/c2jm33199c
- Yao, L., Wang, W., Wang, L., Liang, Y., Fu, J., and Shi, H. (2018). Chemical bath deposition synthesis of TiO<sub>2</sub>/Cu<sub>2</sub>O core/shell nanowire arrays with enhanced photoelectrochemical water splitting for H<sub>2</sub> evolution and photostability. *Sci. Direct* 43, 15907–15917. doi: 10.1016/j.jhydene.2018.06.127
- Yin, Y., Ma, N., Xue, J., Wang, G., Liu, S., Li, H., et al. (2019). Insights into the role of poly(vinylpyrrolidone) in the synthesis of palladium nanoparticles and their electrocatalytic properties. *Langmuir* 35, 787–795. doi: 10.1021/acs.langmuir.8b04032
- Yoon, K. R., Ko, J. W., Youn, D.-Y., Park, C. B., and Kim, D. (2015). Synthesis of Ni-based co-catalyst functionalized W:BiVO<sub>4</sub> nanofibers for solar water oxidation. *Green Chem.* 18, 944–950. doi: 10.1039/C5GC01588J
- Youn, D. H., Park, Y. B., Kim, J. Y., Magesh, G., Jang, Y. J., and Lee, J. S. (2015). One-pot synthesis of NiFe layered double hydroxide/reduced graphene oxide composite as an efficient electrocatalyst for electrochemical and photoelectrochemical water oxidation. *J. Power Sources* 294, 437–443. doi: 10.1016/j.jpowsour.2015.06.098
- Zhang, K., Wang, L., Sheng, X., Ma, M., Jung, M. S., Kim, W., et al. (2016). Tunable bandgap energy and promotion of H<sub>2</sub>O<sub>2</sub> oxidation for overall water splitting from carbon nitride nanowire bundles. *Adv. Energy Mater.* 6:1502352. doi: 10.1002/aenm.201502352
- Zhang, L., Yang, C., Xie, Z., and Wang, X. (2017). Cobalt manganese spinel as an effective cocatalyst for photocatalytic water oxidation. *App. Catal. B Environ.* 224, 886–894. doi: 10.1016/j.apcatb.2017.11.023
- Zhang, M. T., Chen, Z., Kang, P., and Meyer, T. J. (2013). Electrocatalytic water oxidation with a copper(II) polypeptide complex. *J. Am. Chem. Soc.* 135, 2048–2051. doi: 10.1021/ja3097515
- Zhang, P., Zhang, J., and Gong, J. (2014). Tantalum-based semiconductors for solar water splitting. *Chem. Soc. Rev.* 43, 4395–4422. doi: 10.1039/c3cs60438a
- Zhang, R., Ren, X., Shi, X., Xie, F., Zheng, B., Guo, X., et al. (2018). Enabling effective electrocatalytic N<sub>2</sub> conversion to NH<sub>3</sub> by the TiO<sub>2</sub> nanosheets array under ambient conditions. *ACS Appl. Mater. Inter.* 10, 28251–28255. doi: 10.1021/acsami.8b06647
- Zhang, Y., Chen, P., Ma, Y., He, S., and Liu, M. (2009). Acidification and assembly of porphyrin at an interface: counterion matching, selectivity, and supramolecular chirality. *ACS Appl. Mater. Inter.* 1, 2036–2043. doi: 10.1021/am900399w
- Zhang, Y., Zhang, H., Liu, A., Chen, C., Song, W., and Zhao, J. (2018). Rate-limiting o-o bond formation pathways for water oxidation on hematite photoanode. *J. Am. Chem. Soc.* 140, 3264–3269. doi: 10.1021/jacs.7b10979
- Zhao, H., Dai, Z., Xu, X., Pan, J., and Hu, J. (2018a). Integrating semiconducting catalyst of ReS<sub>2</sub> nanosheets into P-silicon photocathode for enhanced solar water reduction. *ACS Appl. Mater. Inter.* 10, 23074–23080. doi: 10.1021/acsami.8b04740
- Zhao, H., Tang, Z., Sun, J., Lowe, S. E., Zhang, L., and Wang, Y. (2018b). Ultrathin nitrogen-doped holey carbon @ graphene bifunctional electrocatalyst for oxygen reduction and evolution reactions in alkaline and acidic media. *Angew. Chem.* 130, 16749–16753. doi: 10.1002/anie.201811573
- Zheng, D., Gao, Z., He, X., Zhang, F., and Liu, L. (2004). Surface and interface analysis for copper phthalocyanine (CuPc) and indium-tin-oxide (ITO) using X-ray photoelectron spectroscopy (XPS). *Spectrosc. Spect. Anal.* 211, 24–30. doi: 10.1016/S0169-4332(02)01333-8
- Zhou, L. L., Fang, T., Cao, J. P., Zhu, Z. H., Su, X. T., and Zhan, S. Z. (2015). A dinuclear copper(II) electrocatalyst both water reduction and oxidation. *J. Power Sources* 273, 298–304. doi: 10.1016/j.jpowsour.2014.09.075
- Zhu, M., Chen, P., and Liu, M. (2011). Graphene oxide enwrapped Ag/AgX (X = Br, Cl) nanocomposite as a highly efficient visible-light plasmonic photocatalyst. *ACS Nano* 5, 4529–4536. doi: 10.1021/nn200088x

**Conflict of Interest Statement:** The authors declare that the research was conducted in the absence of any commercial or financial relationships that could be construed as a potential conflict of interest.

Copyright © 2019 Li, Yang, Tian, Luo, Li, Zhang, Zhou and Xiong. This is an open-access article distributed under the terms of the Creative Commons Attribution License (CC BY). The use, distribution or reproduction in other forums is permitted, provided the original author(s) and the copyright owner(s) are credited and that the original publication in this journal is cited, in accordance with accepted academic practice. No use, distribution or reproduction is permitted which does not comply with these terms.